Bloom, R.; Hondow, N.; Dupont, V.; Twigg, M. V.; Milne, S. J.

Article

Fibrous aluminosilicate catalyst support for hydrogen production by chemical looping steam reforming

Energy Reports

Provided in Cooperation with:
Elsevier

Suggested Citation: Bloom, R.; Hondow, N.; Dupont, V.; Twigg, M. V.; Milne, S. J. (2018) : Fibrous aluminosilicate catalyst support for hydrogen production by chemical looping steam reforming, Energy Reports, ISSN 2352-4847, Elsevier, Amsterdam, Vol. 4, pp. 733-743, https://doi.org/10.1016/j.egyr.2018.10.008

Energy Reports 4 (2018) 733–743

Contents lists available at ScienceDirect

Energy Reports

journal homepage: www.elsevier.com/locate/egyr

Research paper

Fibrous aluminosilicate catalyst support for hydrogen production by chemical looping steam reforming

R. Bloom [a], N. Hondow [a], V. Dupont [a], M.V. Twigg [b], S.J. Milne [a,*]

[a] School of Chemical and Process Engineering, University of Leeds, Leeds LS2 9JT, UK
[b] Twigg Scientific and Technical Ltd, Caxton, Cambridge, CB23 3PQ, UK

HIGHLIGHTS

- Ni/NiO catalyst deposited on novel, low-density fibrous ceramic support.
- Hydrogen production by fixed bed chemical looping steam reforming (CLSR) evaluated.
- Excellent performance when compared to granulated traditional oxygen carrier.
- Possibility of new CLSR reactors designed for distributed H 2 production.

GRAPHICAL ABSTRACT

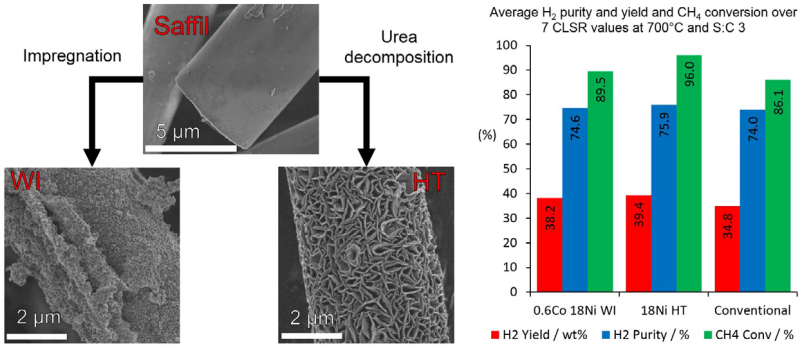

ARTICLE INFO

Article history:
Received 18 July 2018
Received in revised form 30 August 2018
Accepted 18 October 2018
Available online 10 November 2018

Keywords:
Catalyst support
Oxygen carrier
Chemical looping
Steam reforming
Hydrogen

ABSTRACT

Motivated by possible future applications in low pressure drop reactors for hydrogen production by fixed bed chemical looping steam reforming (CLSR), novel high porosity fibrous mats of aluminosilicate fibres have been investigated as a substrate for Ni/Co oxygen carriers (OC's). When compared to granules of a conventional 18 wt% NiO steam reforming catalyst tested over seven redox cycles of CLSR, the fibrous OCs produced by homogeneous chemical precipitation routes increased the average methane conversion by up to 10% and hydrogen yield by up to 5%. All of the OC's could be reduced by a CH_4/H_2O mixture and produced no solid carbon during reforming.

1. Introduction

Scientific consensus on the dangers of anthropogenic climate change has become near irrefutable in recent years, prompting a drive to reduce greenhouse gas emissions from a number of industries. Hydrogen gas is an important bulk chemical that is used primarily in the production of fertilizers and refining of petroleum crudes. It is also considered a strategic, clean alternative to fossil fuel for transport and grid electricity. The industrial production of H_2 as a bulk chemical is currently dominated by steam reforming (SR) of natural gas; a large scale, carbon intensive process that requires centralized production.

Chemical looping steam reforming (CLSR) is a H_2 production technology designed to improve the provision of heat and reduce the burden of H_2 separation in the SR process, thereby reducing carbon dioxide emissions, improving efficiency and potentially allowing decentralized generation and distribution (Protasova and Snijkers, 2016; Adanez et al., 2012; Dueso et al., 2012). Decentralization of H_2 production via smaller scale generation processes can facilitate the use of widely available renewable biomass and waste feedstocks such as biogas, biodiesel, pyrolysis oils, ethanol and glycerol (Cheng et al., 2017). The CLSR process relies on the cyclical

* Corresponding author.
E-mail addresses: marsarbooks@yahoo.co.uk (M.V. Twigg), s.j.milne@leeds.ac.uk (S.J. Milne).

https://doi.org/10.1016/j.egyr.2018.10.008

reduction and re-oxidation of a metal oxide, which is known as an Oxygen Carrier (OC). The OC is cyclically exposed to a reducing fuel/steam atmosphere and an oxidizing air atmosphere in one of two ways: (1) by alternating the fuel/steam mix and air feeds to a single fixed bed reactor or (2) by physically moving the OC between two fluidized bed reactors, each one fed with a continuous stream of fuel/steam or air. In the steam reforming half cycle, the OC is reduced to a catalytically active state by a hydrocarbon fuel/steam flow and serves as the catalyst for the steam reforming of the methane feed (SR, Eq. (1)) and the water gas shift reaction (WGS, Eq. (2)).

$$CH_{4(g)} + H_2O_{(g)} \leftrightarrows 3H_{2(g)} + CO_{(g)} \qquad \Delta H_{298K} = 228\ \text{kJ mol}^{-1} \tag{1}$$

$$CO_{(g)} + H_2O_{(g)} \leftrightarrows CO_{2(g)} + H_{2(g)} \qquad \Delta H_{298K} = -33\ \text{kJ mol}^{-1} \tag{2}$$

Carbon may be formed during this process causing deactivation of the catalyst. Carbon is produced by: thermal cracking (Eq. (3)); CO disproportionation (Eq. (4)); or reduction of CO (Eq. (5)).

$$CH_{4(g)} \leftrightarrows 3H_{2(g)} + C_{(s)} \qquad \Delta H_{298K} = 75\ \text{kJ mol}^{-1} \tag{3}$$

$$2CO_{(g)} \leftrightarrows CO_{2(g)} + C_{(s)} \qquad \Delta H_{298K} = -172\ \text{kJ mol}^{-1} \tag{4}$$

$$CO_{(g)} + H_{2(g)} \leftrightarrows H_2O_{(g)} + C_{(s)} \qquad \Delta H_{298K} = -131\ \text{kJ mol}^{-1} \tag{5}$$

Under the oxidation half-cycle the OC, and any carbon deposited during steam reforming, is oxidized by an air flow in highly exothermic reactions. These reactions provide heat throughout the reactor bed for the subsequent endothermic SR reaction (Protasova and Snijkers, 2016; Adanez et al., 2012).

The choice of OC is therefore integral to the design of the CLSR process. An OC must present high reactivity for the reduction and oxidation reactions involved and maintain that reactivity over extended cycling. It must exhibit high oxygen transfer capacity and favourable thermodynamic properties. The OC should also be readily reduced by a number of fuel mixtures, and act as an effective catalyst for the SR reactions involved in the process. Resistance to attrition and agglomeration is important if the OC is to be used in a fluidized bed reactor, and the cost and complexity of synthesis of the OC must be kept to a minimum (Adanez et al., 2012; Dueso et al., 2012; Rydén and Ramos, 2012; Tang et al., 2015; Noorman et al., 2007; Gayán et al., 2009; Quddus et al., 2013). Moreover resistance to sintering induced degradation is important; low density fibrous mats with minimal numbers of contact points between the fibres may offer advantages in this context.

Many carriers have been tested for use in chemical looping applications but supported transition metals have attracted the most interest (Adanez et al., 2012; Quddus et al., 2013). Metal oxides of iron, nickel, manganese, copper and cobalt have all been used, supported on alumina, zirconia, silica, titania, or bentonite (Adanez et al., 2012; Gayán et al., 2009; Ryu et al., 2001). Nickel when supported on alumina (Ni/α-Al_2O_3 or Ni/γ-Al_2O_3) is by far the most widely researched OC for syngas and H_2 production. This is thanks to strong catalytic activity for the SR reactions, acceptable oxygen transfer capacity and high redox reaction rates at the temperatures encountered in CLSR (Adanez et al., 2012; Tang et al., 2015; Noorman et al., 2007; Quddus et al., 2013; Zafar et al., 2005, 2006; Noorman et al., 2010; de Diego et al., 2008).

The synthesis method used to produce an alumina supported OC must achieve close control of the distribution of the deposited metal oxide and minimize chemical reactions that degrade the catalytic activity (Dueso et al., 2012; Gayán et al., 2009, 2008; Mattisson et al., 2006). In the case of nickel oxygen carriers the formation of spinel nickel aluminate ($NiAl_2O_4$) reduces the amount of NiO (Gayán et al., 2009; Quddus et al., 2013; Mattisson et al., 2006; Dueso et al., 2010): NiO is the more reactive species in redox and in the SR and WGS reactions (Eqs. (1) and (2)) (Noorman et al., 2007; Mattisson et al., 2006; Dueso et al., 2010). It is thus imperative to devise a synthesis procedure that minimizes the formation of $NiAl_2O_4$ and therefore maximizes the proportion of Ni in the form of NiO.

Metal support interactions dictate whether NiO or $NiAl_2O_4$ is formed during synthesis; a strong chemical interaction will produce $NiAl_2O_4$ whereas a weak interaction will produce NiO (Quddus et al., 2013; Zafar et al., 2006). Bolt et al. suggested that there are likely to be two major factors that affect these interactions (Bolt et al., 1998); the crystalline phase of alumina used and the temperature to which the OC's are exposed. Bolt hypothesized that due to its "defect spinel structure" γ-Al_2O_3 facilitates the entry of metal cations (e.g. Ni^{2+}) into its crystal lattice, and therefore γ-Al_2O_3would interact more strongly with the metal species and at a more rapid rate than α-Al_2O_3 during synthesis (Bolt et al., 1998). Additionally if exposed to temperatures above 900 °C, the γ-Al_2O_3 would undergo phase transformation to θ-Al_2O_3 and subsequently α-Al_2O_3 thereby promoting chemical reactions between metal and support (Bolt et al., 1998). These hypotheses were confirmed by a number of studies. Cheng et al. and Matisson et al. found that this strong interaction begins to occur when a Ni γ-Al_2O_3 catalyst is exposed to temperatures exceeding 600 °C and becomes increasingly prevalent above 800 °C (Mattisson et al., 2006; Cheng et al., 1996). In a series of investigations, Dueso et al. (2012) and Dueso et al. (2010). investigated the metal-support reactions between two nickel OC's involving γ-Al_2O_3 and α-Al_2O_3 supports; the α-Al_2O_3OC produced a higher proportion of NiO than the γ-Al_2O_3 OC. This increased proportion of NiO when using α-Al_2O_3 was corroborated by the work by You et al. (2014).

The addition of cobalt has been found to improve the performance of Ni/Al_2O_3 catalysts (Bolt et al., 1998; Hossain et al., 2007; Hossain and de Lasa, 2007). This has been attributed to preferential formation of $CoAl_2O_4$ over $NiAl_2O_4$ spinel due to faster kinetics of the CoO–Al_2O_3 reaction (Bolt et al., 1998). This results in a greater proportion of 'free' NiO, and therefore improved OC performance.

These OC's also offer advantages such as excellent redox cycling durability, strong suppression of carbon formation and stable SR performance attributed to the interactions between the two active metals (You et al., 2014; Hossain et al., 2007; Hossain and de Lasa, 2007; Jin et al., 1998).

Although metal-support interactions have been widely reported, the effect of synthesis method upon homogeneity of metal dispersion is less well discussed. In many of the papers mentioned above, traditional incipient wetness impregnation techniques were used to deposit an active metal upon the support. In this technique, a metal salt solution is introduced to the support and the mixture then dried in order to bring about the deposition of the salt inside the pores of the support. A critical stage in this technique is drying; as the solvent evaporates, the salt is gradually concentrated and deposited. As a result a non-uniform deposition may be expected (Dueso et al., 2010; Zhao et al., 2000). Urea-decomposition is an alternative deposition route which offers superior control of the distribution of catalyst over a substrate. The method relies on the slow decomposition of urea above 90 °C in aqueous media which causes a uniform increase in pH throughout the solution (Tang et al., 2015; Gayán et al., 2009).

In the present work low-density mats of Saffil fibre are investigated as a novel Ni/Co substrate material for CLSR applications. Urea decomposition and wet impregnation deposition routes have been examined. Saffil (catalytic grade) is a fibrous crystalline material consisting of γ-Al_2O_3 (95%) and SiO_2 (5%). The Saffil supported OC's have been evaluated in terms of hydrogen yield and purity, and methane conversion in a fixed bed CLSR process over several redox cycles. The results demonstrate a significant difference in

Table 1
Physical characteristics of the OC's used in the study.

Sample	Metal loaded[a] (wt%)			SSA[b] ($m^2\ g^{-1}$)
	Ni	Co	Ni:Co	
Saffil	–	–	–	106
18Ni WI	17.66	0.00	–	93
0.6Co 18Ni WI	15.97	0.48	33.35	61
1.8Co 18Ni WI	19.29	1.57	12.33	65
18Ni DP	17.31	0.00	–	102
0.6Co 18Ni DP	18.09	0.51	35.61	120
1.8Co 18Ni DP	17.20	1.36	12.65	118
18Ni HT	19.76	0.00	–	117
0.6Co 18Ni HT	18.08	0.50	35.83	118
1.8Co 18Ni HT	17.88	1.46	12.27	115

[a]Quantitative elemental analysis determined by Atomic Adsorption Spectrophotometry (AAS).
[b]Specific surface area determined by Brunauer–Emmett–Teller (BET) analysis of physical adsorption of N_2.

morphology of the deposited metal oxide coating and the corresponding steam reforming performance for OCs manufactured by controlled precipitation reactions as opposed to evaporative wet impregnation.

The motivation for the work was to investigate the feasibility of alternative OCs in CLSR. If high activity in both steam reforming and oxygen transfer, retention of large specific surface area and thermal stability under chemical looping conditions can be demonstrated, the high void spaces in a loose assembly of Saffil supported OCs offers the potential to deliver sufficient residence times with low reactor load. Consequently new small and medium scale hydrogen production processes could be realized in future, catering to distributed feedstocks such as unconventional gases (e.g. shale wells) and biomass products (e.g. large farms, anaerobic digestion plants, biorefineries).

2. Experimental

2.1. Materials and synthesis

The Saffil-supported OC's were synthesized via three methods: Wet Impregnation (WI), Urea Decomposition Precipitation (DP) and Hydrothermal Synthesis (HT). Nickel and cobalt were used in varying quantities providing three different nickel to cobalt ratios. A total of nine OC's were made (summarized in Table 1). A conventional pelletized 18 wt% NiO/α-Al_2O_3 (18 wt% NiO, crystallite size 45 nm (Cheng et al., 2017)) was lightly ground into ~200 μm granules which could be accommodated in the bench top reactor.

2.1.1. Wet impregnation (WI)

Starting reagents were $Ni(NO_3)_2.6H_2O$ (10.8756 g), and for mixed catalysts, $Co(NO_3)_2.6H_2O$ (0.2981 g or 0.9052 g) of purity 99.9% (Fischer Scientific). The cobalt loadings were either 0 wt%, 0.6 wt% or 1.8 wt%. The reagents were dissolved in 250 ml of distilled water, into which 10 g Saffil mat, cut into approximately 5 mm^3 shreds, was introduced. The mixture was placed in a drying oven held at 100 °C for 6 h under an air atmosphere to impregnate the fibres with Ni/Co salts. The resultant material was then calcined at 600 °C for 4 h under an air atmosphere to decompose the Ni/Co nitrates to oxides.

2.1.2. Urea decomposition precipitation (DP)

Experimental conditions for deposition of the catalyst on Saffil were based on those reported in the literature to be optimal for urea based homogeneous precipitation onto porous Al_2O_3 substrates (Zhao et al., 2000). The Ni and Co precursors in the same amounts as in WI were added to water, 250 ml, containing dissolved urea, $CO(NH_2)_2$, (Fischer Scientific) and Saffil to give a molar ratio of 1.7 Ni/Co:Urea. This mixture was placed in a beaker covered with a watch glass and placed in an oven; the temperature was raised from room-temperature at 10 °C min^{-1} to 95 °C for a dwell time of 24 h under an air atmosphere. This allowed for the degradation of urea to raise pH and precipitate Ni/Co hydroxides as per the reaction:

$$CO(NH_2)_2 + 3H_2O \rightarrow 2OH^- + 2NH_{4^+} + CO_2\uparrow \text{ Zhao et al. (2000)} \quad (6)$$

The mixture was then placed in a drying oven for 6 h under an air atmosphere at 100 °C to evaporate any remaining solution, and then calcined at 600 °C for 4 h.

2.1.3. Hydrothermal synthesis (HT)

Starting reagents in the same proportions as for WI and DP but in smaller quantities (4.3502 g of $Ni(NO_3)_2.6H_2O$; 0.1191 g or 0.3621 g of $Co(NO_3)_2.6H_2O$) and a proportionate amount of Saffil were added to 100 ml water into which urea ($CO(NH_2)_2$,) was also added at a molar ratio of 1.7 Ni/Co:Urea. The mixture was transferred to a 125 ml Teflon lined autoclave (Parr Scientific) and placed in a furnace heated at 10 °C min^{-1} to 95 °C and held at this temperature for 24 h. The mixture was transferred from the hydrothermal reactor to a drying oven and heated at 100 °C for 6 h to evaporate any remaining solution, followed by calcination at 600 °C for 4 h.

2.2. Characterization

The morphology and microstructure of the OC's were analysed using a Hitachi SU8230 high performance cold field emission scanning electron microscope (SEM). The samples were affixed to 10 mm aluminium stubs via carbon tape and all samples were carbon coated (thickness 2–3 nm) prior to SEM analysis. The materials heavily charged under the electron beam; therefore low voltage (1–2 kV) and current (0.9 μA) settings were used to reduce this.

The phase composition of the raw support and synthesized OC's were analysed using powder X-ray diffraction (XRD). This was carried out using a Bruker D8 diffractometer with a Cu X-ray tube (λ = 1.5406 Å). A step size of 0.025°, scan speed of 2 s per step and a range of 10–75° 2θ were used. Background determination, peak identification and phase identification were conducted using XPert HighScore Plus analysis software. All samples were ground by pestle and mortar to form a powder prior to analysis.

The nanostructures of the OC's were analysed using an FEI Titan^3 Themis (scanning) transmission electron microscope (TEM) operating at 300 kV and fitted with a high angle annular dark field (HAADF) STEM detector, a Super-X 4-detector energy dispersive X-ray (EDX) analysis system and a Gatan One-View CCD. The EDX analysis was performed using Bruker Espirit software (version 1.9.4). All samples were ground in ethanol and added by pipette onto 400 mesh holey carbon coated Cu TEM grids (Agar Scientific).

Quantitative elemental analysis was conducted with the use of a Varian 240 s Atomic Adsorption Spectrophotometer (AAS). Samples were digested in 10 ml of 1:1 HCl and heated under reflux for 30 min. The solution was then diluted to 250 ml with distilled water. Nickel content was analysed using a wavelength of 352.4 nm and a slit width of 0.5 nm; cobalt was analysed at a 240.7 nm wavelength and a slit width of 0.2 nm.

A Quantachrome Instruments NOVA 2200e was used to determine specific surface area (SSA) via the Brunauer–Emmett–Teller (BET) method. All samples were outgassed at 200 °C for three hours and analysed using N_2 as the adsorbate gas at a temperature in the region of 77 K.

2.3. Chemical looping steam reforming

Chemical looping steam reforming experiments assessed the performance of the Saffil based OC's in comparison to the conventional SR catalyst (granulated) in the CLSR process. The experiments consisted of a SR half-cycle and an oxidation half-cycle. The SR half-cycle exposed the various OC's to CH_4 and H_2O under N_2 carrier gas, chemically reducing the OC's as well as performing steam reforming. The carrier gas was used to enable elemental balances and to reach the minimum flow rates required by the analyser for accurate measurements. Oxidation was induced in the half-cycle of air-exposure.

Appropriate conditions for chemical looping experiments were chosen by calculating chemical equilibrium compositions at assigned temperatures and pressures using the computer program CEA (Chemical Equilibrium with Application) developed by NASA Lewis Research Centre (McBride and Gordon, 1994). Conditions of 700 °C and a molar steam to carbon ratio (S:C) of 3 were found to maximize the equilibrium methane conversion and provide high hydrogen yield and purity while minimizing solid carbon deposition and steam flows.

The reactor set-up used in the chemical looping experiments is shown in Fig. 1. CH_4, H_2 and N_2 (BOC, purity 99.995%) and on-site compressed air were used as reactant gases. Mass flow controllers (Bronkhorst EL-FLOW, range 0.1–180 sccm) set the flow rate of CH_4 and H_2 whereas N_2 and air were controlled by electric rotameters (Bronkhorst MASS-VIEW, range 0–2000 sccm). A programmable syringe pump was used to introduce distilled water into the heated zone of the reactor to satisfy the S:C required for each experiment. The 316 stainless steel (SS) reactor had an inside diameter of 13.2 mm and a length of 750 mm of which the bottom 500 mm was heated using a vertical tube furnace (Elite Thermal systems TSVH12/30/450) controlled by a temperature controller (Eurotherm 3216). Additionally a second K-type thermocouple was placed adjacent to the bottom basket and was used to monitor temperature in the catalyst bed to ensure the desired temperature was reached in each experiment.

In each experiment the reactor was loaded with 2 g of OC. The bed volume was 12.5 cm^3 and consisted of 10 stainless steel mesh baskets in which the OC's were held. These baskets were placed in the reactor by resting on a small steel bar welded across the tube. Given the difference in bulk density between the two catalysts (conventional 18 wt% NiO was ~1 g cm^{-3}, the Saffil OC's were ~0.2 g cm^{-3}) the conventional SR catalyst used for comparison purposes was diluted with silica sand to increase the bed volume to that of the Saffil catalyst.

As the analysers used in the apparatus were highly sensitive to water, a condenser (jacketed heat exchanger using a cooling fluid consisting of 1:1 mix of water and ethylene glycol chilled to 2 °C) and a moisture trap (silica gel) were used to remove water prior to gas analysis. The outlet composition of the remaining gases was recorded in vol% every 5 s by an ABB Advanced Optima analyser using three modules; Uras 14 (CO, CO_2 and CH_4 measured by infrared adsorption), Caldos 15 (H_2 via thermal conductivity), and Magnos 106 (O_2 via paramagnetic analysis).

All experiments were conducted at 700 °C with S:C = 3, a N_2 flow rate of 1000 sccm, CH_4 flow rate of 111 sccm and liquid H_2O flow rate of 0.25 sccm. The experiments were conducted via the following procedure. (1) The reactor was heated at 10 °C/min to 700 °C under a flow of 1000 sccm N_2. (2) A mixture of 5 vol% H_2 in N_2 flowed through the catalyst bed at 1000 sccm to reduce the catalyst: reduction was inferred from a rise in the outlet concentration of H_2 to 5 vol%). This ensured that the catalyst was in the reactive metal form rather than the non-catalytically active oxide phase. (3) The reactor was purged with N_2 until H_2 was no longer present in the outlet. (4) The initial SR cycle was then performed by switching on the water feed to pump water into the reactor. When water contacts the reduced catalyst as steam, H_2 is formed via oxidation of the catalyst (water splitting); when this was detected by the analysers, a flow of 111 sccm CH_4 was added to the N_2 flow resulting in a total flow of 1111 sccm of reactant gas at 10 vol% CH_4. This SR regime was continued for 20 min. (5) The CH_4 and water flows were switched off and the reactor purged with N_2 for 5 min. (6) The N_2 flow was switched off and the Air flow set to 1000 sccm for 5 min; in order to oxidize the catalyst. (7) The reactor was then purged for 5 min under 1000 sccm N_2. (8) The water and CH_4 flows were switched on again and reduction of the catalyst occurred: the reduced catalyst then promoted SR and steps 5–8 were repeated until the catalyst had been reduced and oxidized 7 times.

The outputs of the chemical looping experiments were defined by the following equations:

$$H_2 Yield = \left(\frac{\dot{n}_{H_2,out} * \overline{W}_{H_2}}{\dot{n}_{CH_4,in} * \overline{W}_{CH_4}} \right) \times 100\% \quad (7)$$

$$H_2 Purity = \left(\frac{x_{H_2,out}}{x_{CO,out} + x_{CO_2,out} + x_{CH_4,out} + x_{H_2,out}} \right) \times 100\% \quad (8)$$

$$CH_4\ Conversion, X_{CH_4} = \left(\frac{\dot{n}_{CH_4,in} - \dot{n}_{CH_4,out}}{\dot{n}_{CH_4,out}} \right) \times 100\% \quad (9)$$

$$H_2O\ Conversion, X_{H_2O} = \left(\frac{\dot{n}_{H_2O,in} - \dot{n}_{H_2O,out}}{\dot{n}_{H_2O,out}} \right) \times 100\% \quad (10)$$

$$r_{red}, OC = \dot{n}_{dry,out} \left(x_{CO,out} + x_{CO_2,out} + x_{O_2,out} \right) - \dot{n}_{H_2O,in} X_{H_2O} \quad (11)$$

Under both half cycles, molar flow rate of gas component i ($\dot{n}_{i,out}$) was defined as the dry gas mol fraction in the gas products x_i measured online, multiplied by $\dot{n}_{dry,out}$, the molar flow rate of total dry outlet gas from the nitrogen balance. ($\dot{n}_{dry,out}$) was estimated using a nitrogen balance. During the methane/steam feed half cycle, methane conversion and the carbon balance error (where 100% results in a perfect balance) were estimated using a carbon balance. Water conversion was then estimated using a hydrogen balance. Finally, the rate of OC reduction (r_{red}, OC) was estimated with the use of an additional oxygen balance. Total moles of metal oxide reduced over a given time were obtained from a time integration of the rate formula over the duration of the methane/steam feed. In-depth discussion of the elemental balances can be found elsewhere for a generic $C_nH_mO_k$ fuel (Pimenidou et al., 2010). For the air feed half cycle, a carbon balance would have determined if any carbon was present on the OC, as it would have oxidized to CO or CO_2, but it will be seen that neither gases were detected during the air feeds. An oxygen balance then determined the rate of Ni oxidation, and from its integration over time, the moles of Ni oxidized during air feed.

3. Results and discussion

3.1. Material synthesis and characterization

The nominal and chemically analysed metal loadings of the OC's were generally in good agreement, Table 1, confirming the validity of the synthesis methods employed. X-ray powder diffraction showed NiO peaks and broad peaks of γ-Al_2O_3 (ICDD 00-010-0425) and SiO_2(ICDD 01-080-6157) from the Saffil support, Fig. 2 (Peng et al., 2001). No CoO was detected in the mixed catalyst samples, as its concentration fell below the XRD detection limit. Important in the context of OC performance, any $NiAl_2O_4$ was also below XRD detection limits (< 5%).

Scanning electron microscopy of uncoated Saffil indicated fibre diameters in the range 2–5 μm, Fig. 3a. Examination of the coated fibres showed the WI method was the least effective deposition route, giving erratic distributions of the metal oxide phase, Fig. 4a–b; some fibres were completely covered in a layer of densely

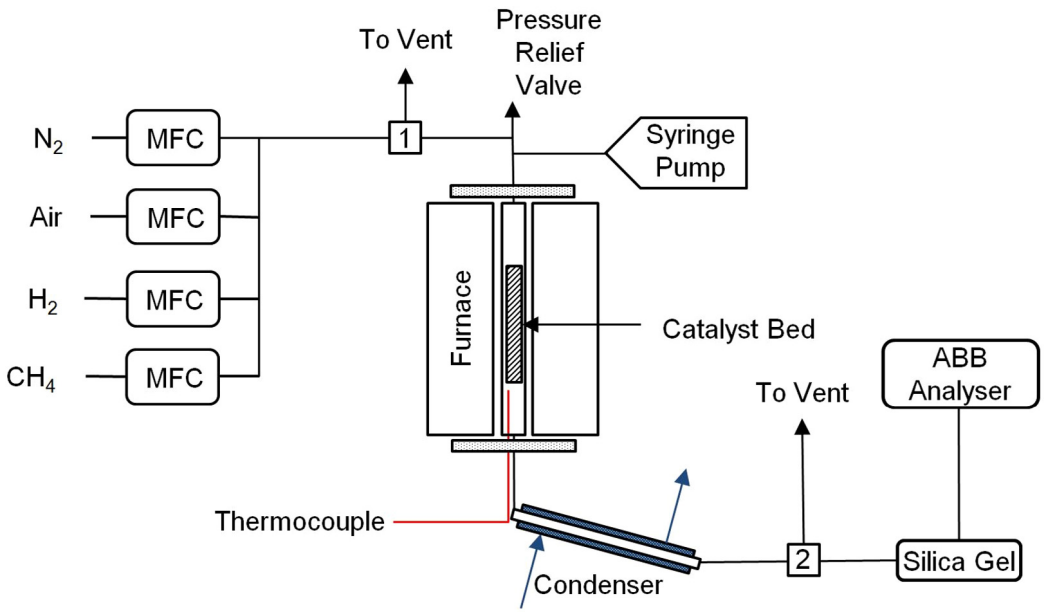

Fig. 1. Reactor set-up for chemical looping experiment.

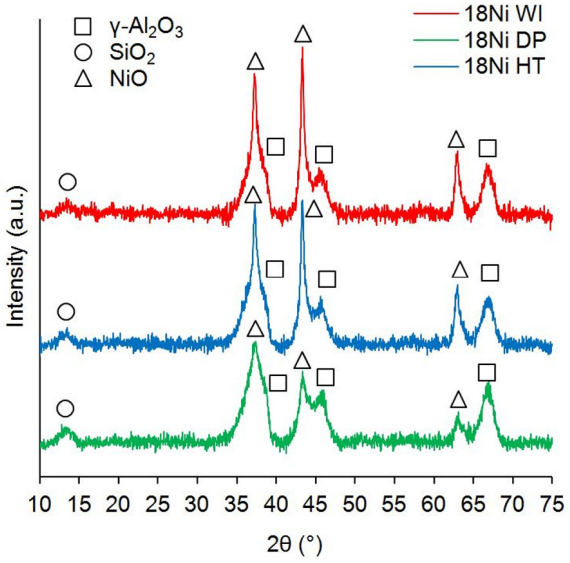

Fig. 2. XRD patterns of 18Ni OC's synthesized via WI, DP and HT methods.

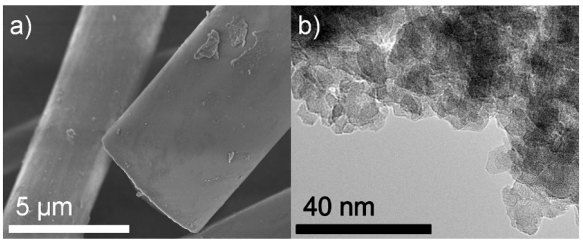

Fig. 3. SEM (a) and TEM images (b) of the as-received Saffil fibres.

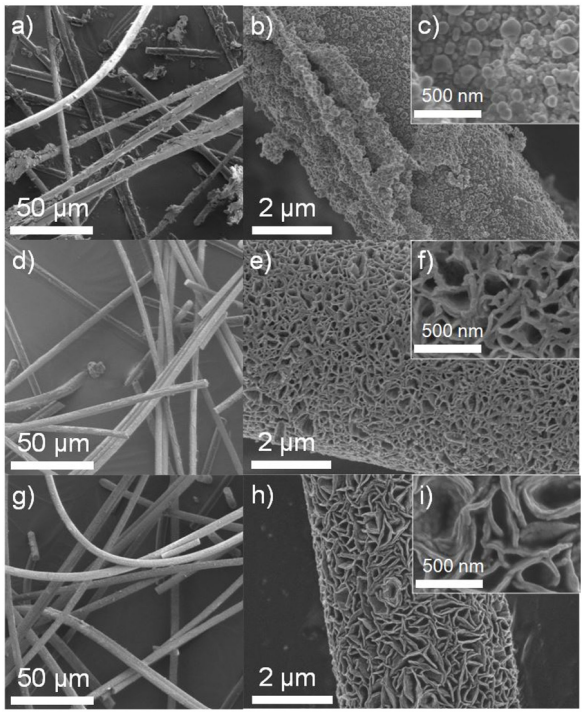

Fig. 4. SEM images of 18Ni WI (a, b and c), 0.6Co 18Ni DP (d, e and f) and 0.6Co 18Ni HT (g, h and i).

packed metal oxide particles and there were examples of micron sized agglomerates on top of some regions of the coating. In terms of crystallite morphology, the WI route led to coatings composed of round, nodular crystallites with a wide size distribution, including some up to ∼ 100 nm in size, Fig. 4c. This variability is typical of a wet impregnation method as during drying a range of precipitation and growth conditions exist leading to non-uniformity in coating integrity and particle sizes (Neimark et al., 1981).

The DP and HT synthesis routes each gave more uniform distributions of the deposited material with little or no evidence of uncoated areas. Fig. 4d and e show SEM images for DP. Micrographs of HT samples appear in Fig. 4g–i. Both coatings appeared as a series of folded layers, possibly representing a series of interconnected platelet crystallites, with edges normal to the surface of the fibres. The network of folded 'ridges' with solid walls up to ∼100 nm in width framed void spaces with lateral dimensions of up to ∼

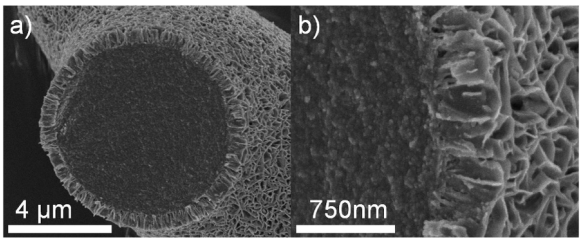

Fig. 5. SEM images of 1.8Co 18Ni DP (a and b).

400 nm for DP and to 500 nm for the less densely folded HT coatings.

The addition of Co seemed to have little effect on the morphology of the catalysts produced by any of the synthesis routes. Fig. 5a and b show typical SEM cross sections of a DP sample revealing a metal oxide layer thickness of ∼ 500 nm. The ridge structure extends from the outer surface to the fibre-interface indicating a progressive growth of the metal oxide layer perpendicular to the fibre surface.

The BET specific surface areas of the uncoated Saffil fibre and the synthesized OC's are shown in Table 1. The as-received Saffil fibres had a SSA of 106 m^2 g^{-1}. The deposition of NiO by the WI method reduced the SSA compared to the Saffil substrate. By contrast, the HT and DP OC's generally exhibited a higher SSA, with one exception, the 18Ni DP sample (102 m^2 g^{-1}). The OC's via the HT route produced the most consistent SSA results, with all HT OC's showing an SSA in excess of 115 m^2 g^{-1} and varying in SSA by only ∼5 m^2 g^{-1}. There appeared to be no effect on SSA from cobalt doping. The increase in measured SSA from DP and HT synthesis routes, relative to WI, is consistent with the porous coatings disclosed by SEM (Fig. 3).

Transmission electron microscopy of uncoated Saffil fibres had indicated a crystallite size of approximately 4–6 nm, Fig. 3b. TEM of the 18Ni WI sample, Fig. 6a and b, revealed rounded particle profiles consistent with the nodular structures observed by SEM (Fig. 4b and c). The estimated average size of these crystals was 73 nm, with a range from 20 nm to 150 nm (based on 50 crystals measured). TEM images of the coatings in DP and HT samples revealed that the folds (wall thickness ∼ 100 nm) were composed of a sub structure of sub 10 nm crystallites, Fig. 6c–e. Some detached fibril-like nanoparticles were also evident. Corresponding HAADF STEM images and EDX maps are shown in Fig. 7. The location of the interface between fibre-and coating was located from EDX analysis (white and black arrows inset); from this the depth of Ni coating could be evaluated. The 18Ni WI sample indicated a deposited layer of < 200 nm whilst the coatings in the DP and HT samples were thicker at ∼ 300 nm and ∼ 400 nm respectively, consistent with the thickness estimated from SEM section (Fig. 5a). Analysis of electron diffraction patterns yielded d-spacings in agreement with the XRD analysis conducted earlier that was consistent with a NiO coating (refer to Figure S1 and Table S1).

Aluminium was detected from TEM-EDX co-existing with Ni (**and Co)** even at the outermost surface of the metal oxide coating (Area 1, Fig. 7, Table 2 and Figure S2). Table 2, shows the semi quantitative analysis of Areas 1 and 2 in Fig. 7a–i. The quantity of Al at the surface of the deposited layer (Area 1) is least in the WI sample (15 at. %) and highest in the HT sample (35 at. %). Corresponding EDX spectra are shown in Figures S3–S5.

The presence of Al at the surface of the deposited layer may arise from partial dissolution of Saffil during the chemical treatments involved in synthesizing the OC's. It has been reported that addition of nickel and cobalt nitrate to water can cause some dissolution of pure powdered γ-Al_2O_3 supports due to the change in pH (Espinose et al., 1995). In the present work, the Al detected

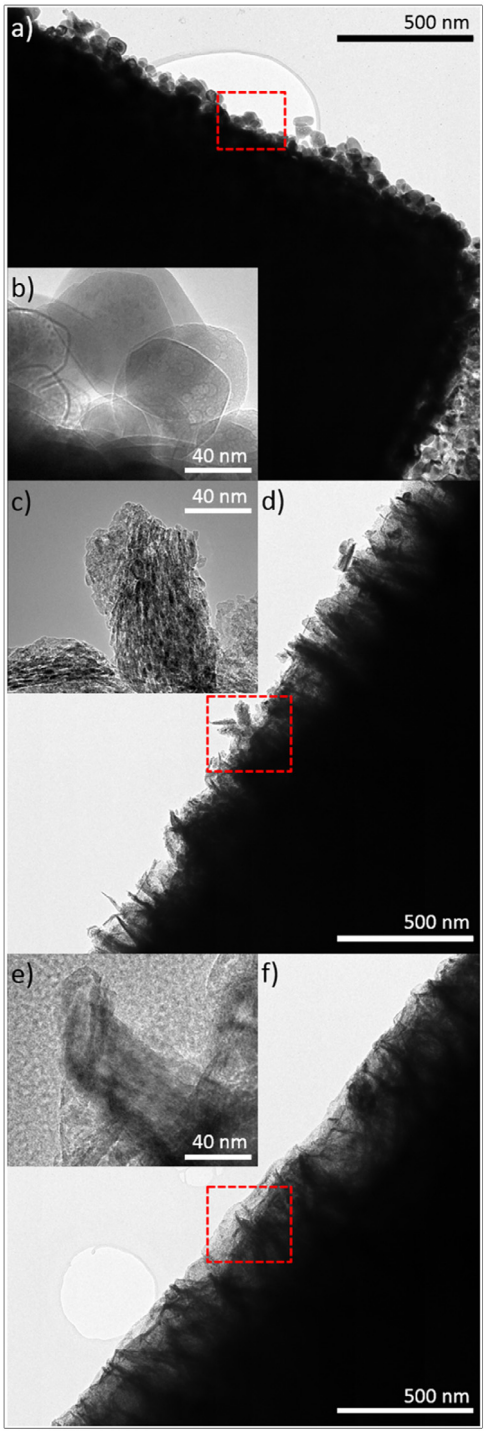

Fig. 6. TEM images of the 18Ni WI (a and b), 18Ni DP (c and d) and 0.6Co 18Ni HT (e and f) samples. Figures a, c and e are higher magnification images of the areas highlighted.

by TEM-EDX in the catalyst phase suggests some co-precipitation of Ni^{2+}, Co^{2+} and Al^{3+} species ions occurred. This sequence may account for the very unusual 'honeycomb' structure to the DP and HT coatings on Saffil, as identified by SEM (Fig. 4). The Saffil fibres were only in contact with the precursor solution for a limited amount of time in the WI method (i.e. until the precursor solution had evaporated), thereby severely limiting any Saffil dissolution. The chemical conditions in DP, and more so HT synthesis methods are expected to promote increased Saffil dissolution.

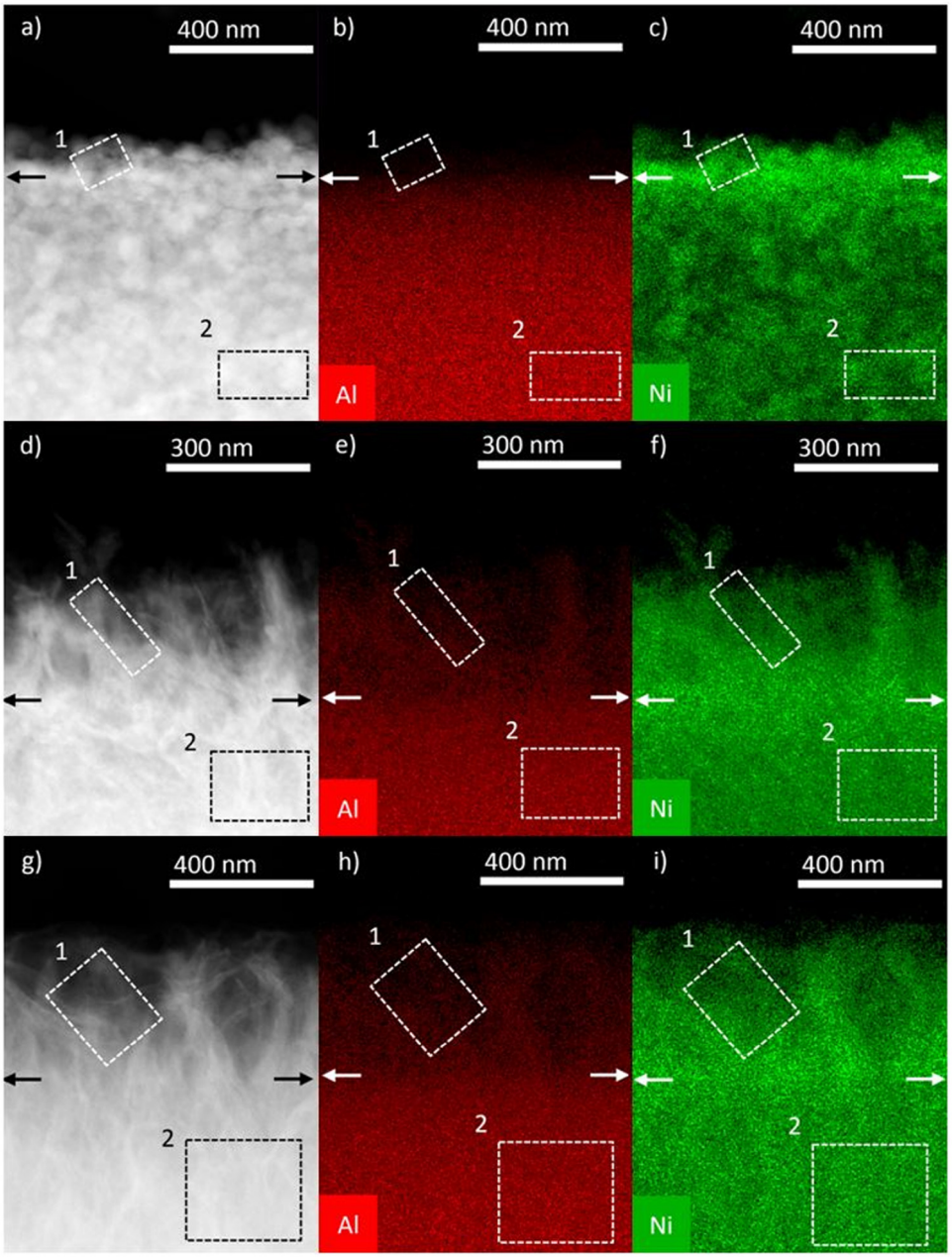

Fig. 7. TEM-EDX mapping of the 18Ni WI (a, b and c), 18Ni DP (d, e and f) and 0.6Co 18Ni HT (g, h and i) samples with highlighted areas showing the location of semi-quantitative analysis.

Table 2
Semi-quantitative EDX elemental analysis.

Sample	Area 1[a]		Area 2[a]	
	Ni (%)	Al (%)	Ni (%)	Al (%)
18Ni WI	85	15	28	72
18Ni DP	72	28	31	69
0.6Co 18Ni HT	65	35	28	72

[a]Where Area 1 and 2 refer to the highlighted areas in Fig. 7a–i.

We tentatively ascribe the morphology of the coatings from DP and HT methods to a formation mechanism involving layered intermediate phases such as double layer hydroxides, DLHs. The soluble Al species and the presence of carbonate ions from urea decomposition, along with Ni/Co ions would provide a solution environment from which DLHs, $[M^{2+}_{1-x}M^{3+}_{x}(OH)_2][CO_{3x/2}]\cdot mH_2O$ could form (Li et al., 2012; Feng et al., 2009; Xu et al., 2015; Christensen et al., 2006).

The reactions may be represented as follows in Eqs. (12)–(15).

$$Al_2O_3 + 3H_2O + 2OH^- \rightarrow 2[Al(OH)_4]^- \quad (12)$$

$$Ni^{2+} + 2OH^- \rightarrow Ni(OH)_2 \quad (13)$$

$$CO_2 + H_2O \rightarrow CO_3^{2-} + 2H^+ \quad (14)$$

$$(1-x)Ni(OH)_2 + xAl(OH)_{4-} + x/2{CO_3}^{2-} \rightarrow [Ni_{1-x}{Al^{3+}}_x(OH)_2]^{x+} ({CO_3}^{-2})_{x/2} + 2xOH^- \quad (15)$$

Double layer hydroxides, formed in this case from Ni and Al ions (the latter from dissolution of Saffil fibres) as represented by Eqs. (12)–(15), typically crystallize with a characteristic platelet morphology due to their hexagonal crystal structure and low surface

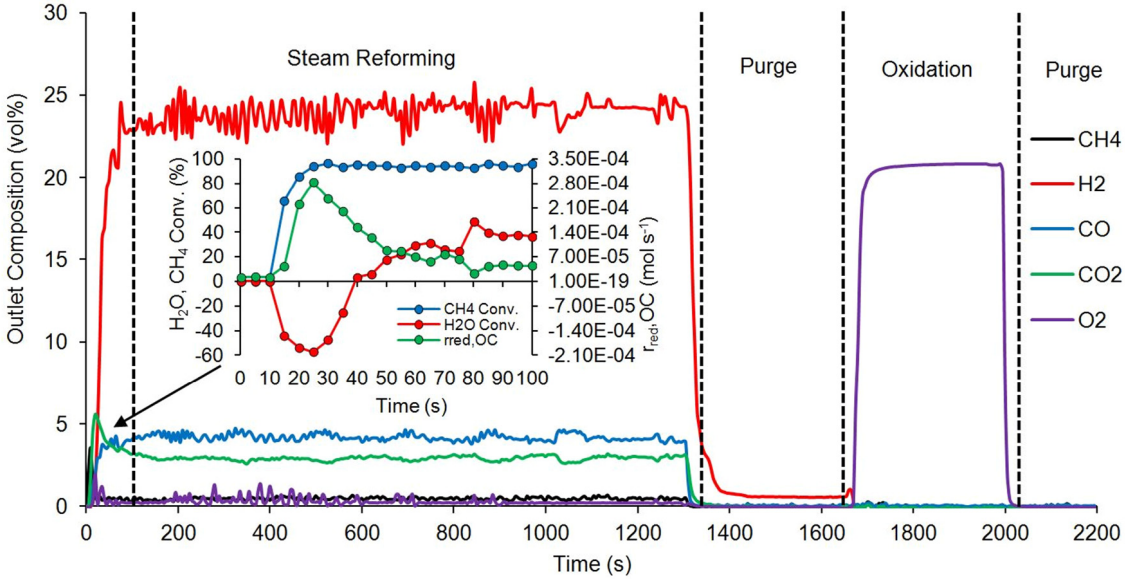

Fig. 8. Dry outlet composition during the 7th cycle of CLSR using 0.6Co 18Ni DP catalyst at 700 °C and S:C 3 as representative of a typical CLSR cycle. Shows reduction of catalyst, steam reforming and oxidation of catalyst.

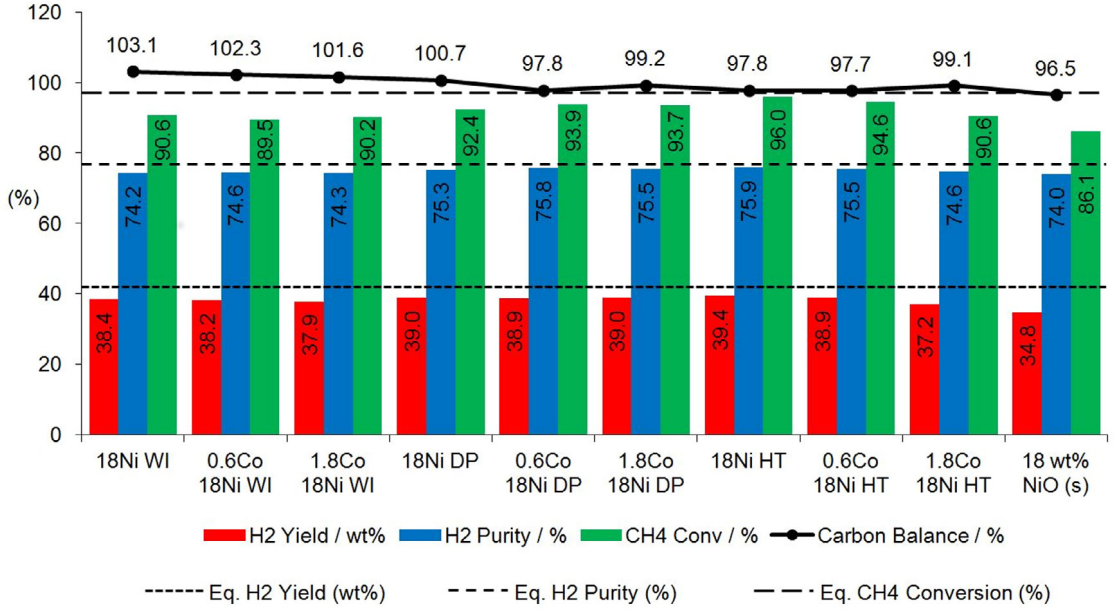

Fig. 9. Average H_2 purity and yield and CH_4 conversion over 7 CLSR cycles compared with equilibrium values at 700 °C and S:C 3:. "18 wt%NiO (s)" represents the 18 wt% NiO SR catalyst when used with quartz sand as a packing material to produce equal catalyst bed volume (more detail in the experimental section).

energy of *ab* crystal planes. For example Li et al. report platelet DLH crystals from urea derived synthesis of Ni/Mg catalysts on alumina particles that have broad similarities to the DP and HT product morphologies (Li et al., 2012). A high lateral growth rate of anisotropic LDH crystals, perpendicular to the Saffil support may in part explain the ridged, folded structure observed in DP and HT samples. However a future dedicated crystal growth study would be required to fully understand the growth mechanism.

3.2. Chemical looping steam reforming

The outlet composition for the Saffil OC's during the SR and the oxidation half cycle is shown in Fig. 8 for a DP sample, and is representative of all the OC's tested. The inset graph in Fig. 8 shows the CH_4 and H_2O conversions and the rate of NiO reduction (r_{red},OC) derived from Eqs. (9)–(11) during the first 100 s of the SR half-cycle.

The onset of OC reduction is clearly shown in the inset figure: r_{red},OC increased after 10 s and peaked at 25 s coinciding with a rapidly decreasing negative H_2O conversion, and an increasingly positive CH_4 conversion. Negative H_2O conversion signifies a production of H_2O, this coupled with an increase in CH_4 conversion implies that the global reduction of the OC through complete combustion (Eq. (16)) was favoured over other likely reduction reactions (Eqs. (17), (18) or (19)). After 25 s, an abundance of the reduced OC caused the initiation of the SR and WGS reactions (Eqs. (1) and (2)) thereby consuming H_2O and thus increasing the H_2O conversion.

As the reduction neared completion, r_{red},OC decreased, while H_2O conversion increased and reached steady state as the SR and

Table 3
Estimated average maximum rate of reduction over 7 CLSR cycles at 700 °C and S:C 3.

Sample	Maximum r_{red},OC (mol s^{-1})
18Ni WI	2.08×10^{-4}
18Ni DP	1.91×10^{-4}
18Ni HT	2.06×10^{-4}
18Ni Average	2.02×10^{-4}
0.6Co 18Ni WI	2.17×10^{-4}
0.6Co 18Ni DP	2.08×10^{-4}
0.6Co 18Ni HT	2.26×10^{-4}
0.6Co 18Ni Average	2.17×10^{-4}
1.8Co 18Ni WI	2.32×10^{-4}
1.8Co 18Ni DP	2.18×10^{-4}
1.8Co 18Ni HT	2.23×10^{-4}
1.8Co 18Ni Average	2.24×10^{-4}
18 wt% NiO (s)	2.14×10^{-4}

WGS reactions dominated.

$$CH_{4(g)} + 4NiO_{(s)} \leftrightarrows 4Ni_{(s)} + CO_{2(g)} + 2H_2O_{(g)}$$
$$\Delta H_{298K} = 135 \text{ kJ mol}^{-1} \quad (16)$$

$$CH_{4(g)} + NiO_{(s)} \leftrightarrows Ni_{(s)} + CO_{(g)} + 2H_{2(g)} \qquad \Delta H_{298K} = 213 \text{ kJ mol}^{-1} \quad (17)$$

$$CO_{(g)} + NiO_{(s)} \leftrightarrows Ni_{(s)} + CO_{2(g)} \qquad \Delta H_{298K} = -48 \text{ kJ mol}^{-1} \quad (18)$$

$$H_{2(g)} + NiO_{(s)} \leftrightarrows Ni_{(s)} + H_2O_{(g)} \qquad \Delta H_{298K} = -15 \text{ kJ mol}^{-1} \quad (19)$$

Fig. 8 shows no CO_2 or CO peaks during the oxidation half cycle, a result shown across all the OC's' tested. This suggests the absence of complete or partial oxidation of solid carbon

(Eqs. (20) and (21)), and implies a lack of carbon deposition during reduction and steam reforming, thus oxidation of the OC was favoured (Eq. (22)).

$$C_{(s)} + O_{2(g)} \leftrightarrows CO_{2(g)} \qquad \Delta H_{298K} = -393 \text{ kJ mol}^{-1} \quad (20)$$

$$C_{(s)} + 0.5O_{2(g)} \leftrightarrows CO_{(g)} \qquad \Delta H_{298K} = -110 \text{ kJ mol}^{-1} \quad (21)$$

$$2Ni_{(s)} + O_{2(g)} \leftrightarrows 2NiO_{(s)} \qquad \Delta H_{298K} = -468 \text{ kJ mol}^{-1} \quad (22)$$

Table 3 shows the maximum rate of OC reduction (maximum r_{red},OC). The synthesis method did not have a pronounced effect on the maximum rate of reduction (Table 3), however the maximum r_{red},OC increased slightly with decreasing Ni:Co ratio. All of the equations used to calculate these factors are available elsewhere (Pimenidou et al., 2010).

The average H_2 purity and yield and CH_4conversion over 7 CLSR cycles for all 9 OC's is compared to the standard 18 wt% NiO catalyst and equilibrium values shows an error < 5% in the carbon balance between the molar flows of carbon in and out of the reactor across all experiments, indicating accuracy in the measurements and elemental balance analysis.

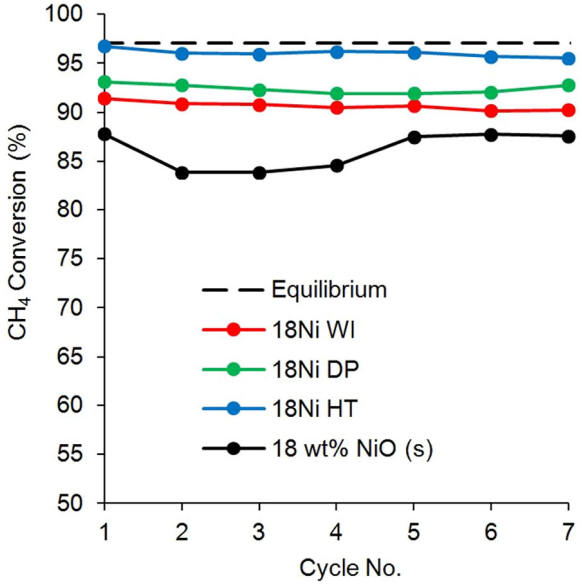

Fig. 10. CH_4 conversion over 7 redox cycles compared with equilibrium values at 700 °C and S:C 3.

All of the Saffil OC's presented an improvement in terms of average CH_4 conversion and H_2 yield over the conventional 18 wt% NiO SR catalyst, Fig. 9, Table 4. The 18Ni HT OC was the most effective, returning a 9.9% improvement in CH_4 conversion and a 4.6% improvement in H_2yield. The other Saffil OC's improved CH_4 conversion by between 3.4% and 8.5% while H_2yield was improved by 3.1% to 4.2%. H_2 purity was largely unchanged.

The CH_4 conversion per cycle over the 7 CLSR test cycles is shown in Fig. 10 and indicates that the performance of the Saffil OC's was stable and consistently superior to the conventional 18 wt% NiO catalyst (in granulated form), with HT having optimum performance, Table 4. The H_2 yield and purity performance over 7 cycles are shown in Figure S6 and show similar enhancements in the Saffil OC's.

There was no measurable difference in performance of OCs modified by cobalt. Additions of Co to Ni/Al_2O_3 have been reported by others to improve steam reforming performance by suppressing $NiAl_2O_4$ spinel formation (Hossain and de Lasa, 2007). A $NiAl_2O_4$ phase is normally formed during high temperature heat-treatments, thereby reducing the amount of available Ni catalyst. The absence of any effect of Co on steam reforming performance in the present work may relate to the milder heat-treatment schedules for OC synthesis and chemical looping which minimizes spinel formation—indeed no spinel phase was identified by X-ray or electron diffraction in any OC.

Table 4
H_2 purity and yield and CH_4 conversion in the 1st and 7th CLSR cycles. Average refers to the mean H_2 purity and yield and CH_4 conversion over all 7 cycles tested.

Sample	H_2 Yield (wt%)			H_2 Purity (%)			CH_4 Conversion (%)		
	1st Cycle	7th Cycle	Average	1st Cycle	7th Cycle	Average	1st Cycle	7th Cycle	Average
18Ni WI	38.73	38.03	38.45	74.59	73.88	74.16	91.37	90.21	90.64
0.6Co 18Ni WI	40.75	36.98	38.19	75.34	74.47	74.58	91.11	88.63	89.51
1.8Co 18Ni WI	39.22	37.07	37.90	75.43	73.69	74.32	92.71	89.92	90.21
18Ni DP	40.50	38.60	38.97	75.87	75.28	75.31	93.07	92.75	92.39
0.6Co 18Ni DP	42.22	37.05	38.86	76.32	75.26	75.82	95.13	93.05	93.86
1.8Co 18Ni DP	40.94	37.27	39.00	76.65	74.99	75.47	94.94	93.01	93.69
18Ni HT	42.74	38.03	39.40	76.60	75.68	75.87	96.74	95.53	96.05
0.6Co 18Ni HT	41.21	37.87	38.88	76.66	75.16	75.54	95.70	94.26	94.63
1.8Co 18Ni HT	40.06	36.51	37.18	76.00	74.23	74.65	93.09	89.85	90.59
18 wt% NiO (s)	36.41	37.04	34.79	75.04	74.48	74.04	87.77	87.56	86.13

In summary, the synthesis of Saffil supported OC's via decomposition of urea (DP and HT) rather by simple liquid evaporation (WI) gives superior CLSR performance. The differences in the H_2 yield and CH_4 conversion can be explained by the lower crystallite size, improved coating uniformity and more open texture. These factors are known to be important in conventional non-fibrous Ni/γ-Al_2O_3 catalysts (Christensen et al., 2006; Ashok et al., 2008; Lucrédio and Assaf, 2006; Song et al., 2013). Reduced particle size results in a lower diffusional resistance to mass transfer between products and reactants in heterogeneous catalysis; the porous structure of the coating identified by SEM will aid gas diffusion, as will the relatively lose packing of the fibres. The role of any incorporated Al on the performance of the OC's is uncertain at this stage.

The low density Saffil OC's developed in this project represent a different type of fibre-based catalyst to the densely packed fibre beds traditionally used for catalytic combustion of methane in space heating using platinum group metals (Radcliffe and Hickman, 1975; Trimm and Lam, 1980b,a) which are currently receiving widespread interest for used in microchannel reactors for the rapid production of H_2 for use in hydrogen fuel cells (Reichelt et al., 2014; Zhou et al., 2015).

The performance comparisons highlight that for a given catalyst mass and volume, Ni/Co fibrous OC's offer significant advantages over traditional catalysts in fixed bed CLSR. Furthermore the low density fibrous OC's may provide other benefits for fixed bed processes. The low-density Saffil OC's present a high surface area to volume ratio and high void fraction in the catalyst bed leading to an excellent compromise between mass transfer for the catalytic reactions and pressure drop through the bed. Additionally they are easily manipulated into various shapes and have a high thermal stability (Reichelt et al., 2014; Zhou et al., 2015; Reichelt and Jahn, 2017; Sadamori, 1999). These factors may prove beneficial to fixed bed CLSR processes, a research field in which fibre catalysts have not been applied. The lower thermal inertia offered by a less dense catalyst in conjunction with the reduction in diffusional resistance potentially allows fast and homogeneous heat provision during oxidation for the endothermic SR reactions allowing for efficient production of H_2 through the SR reactions. Further research is required to establish if these promising features can indeed facilitate a change in CLSR reactor geometry suited to small and medium scale hydrogen production.

4. Conclusions

Ni/Co fibrous oxygen carriers (OC's) have been fabricated utilizing low density mats of a polycrystalline alumina/silica fibre support (Saffil). The performance of oxygen carriers deposited on Saffil by urea homogeneous precipitation in chemical looping steam reforming was equal or better than the commercial 18 wt% NiO catalyst (in granulated form). The Saffil based OC's synthesized in this work showed improved average values of methane conversion and hydrogen yield over the tested seven redox cycles. All of the OC's were reduced by the fuel steam mixture and produced no solid carbon during reforming. Moreover the process advantages of fibre catalysts including high malleability, thermal stability, high surface to volume ratio and void fraction indicate that fibrous catalysts are a promising alternative to conventional catalysts in fixed bed chemical looping steam reforming. Future work will explore the long-term stability and durability of these fibrous OC and explore the kinetics and mass transfer properties associated with reduction and oxidation to further examine their suitability for CLSR in comparison to commercial pelletized catalysts.

Nomenclature	
OC	Oxygen carrier
SR	Steam reforming
CLSR	Chemical looping steam reforming
WI	Wet Impregnation
DP	Urea decomposition-precipitation
HT	Hydrothermal DP
LDH	Layered double hydroxide
SEM	Scanning electron microscopy
TEM	Transmission electron microscopy
EDX	Energy dispersive X-ray analysis
BET	Brunauer–Emmett–Teller
SSA	Specific surface area
XRD	X-ray diffraction
HAADF	High angle annular dark field
AAS	Atomic adsorption Spectrophotometry
S:C	Molar steam to carbon ratio
SS	Stainless steel
$\dot{n}_{i,out}$	dry moles in the reactor outlet of species i
$\dot{n}_{i,in}$	dry moles in the reactor inlet of species i
$x_{i,out}$	vol % in the reactor outlet of species i
$x_{i,in}$	vol % in the reactor inlet of species i
$\overline{W}_i$	Molar mass of species i
X_i	Conversion of species i
r_{red}, OC	Rate of OC reduction (mol s^{-1})

Acknowledgements

Thanks to Jenny Forrester for her assistance with XRD analysis and to Stuart Micklethwaite for his assistance during SEM imaging. This work was supported by the EPSRC via the Low Carbon Technologies Doctoral Training Centre (EP/G036608/1) and the UKCCSRC via the Call 2 Capture Projects (UKCCSRC-C2-181). Further thanks must be extended to Jonathan Cross and Unifrax Ltd for supplying the CG Saffil material and for their input into this project.

Conflict of interest

None.

Appendix A. Supplementary data

Supplementary material related to this article can be found online at https://doi.org/10.1016/j.egyr.2018.10.008.

References

Adanez, J., Abad, A., Garcia-Labiano, F., P. Gayan, P., L.F. de Diego, L.F., 2012. Progress sein Chemical-Looping Combustion and Reforming technologies. Prog. Energy Combust. Sci. 38, 215–282. http://dx.doi.org/10.1016/j.pecs.2011.09.001.

Ashok, J., Subrahmanyam, M., Venugopal, A., 2008. Hydrotalcite sestructure derived Ni-Cu-Al catalysts for the production of H_2 by CH_4 decomposition. Int. J. Hydrogen Energy 33, 2704–2713. http://dx.doi.org/10.1016/j.ijhydene.2008.03.028.

Bolt, PH., Habraken, FHPM., Geus, JW., 1998. Formation seof Nickel, Cobalt, Copper, and Iron Aluminates from α- and γ-alumina supported oxides: A Comparative Study. J. Solid State Chem. 135, 59–69. http://dx.doi.org/10.1006/jssc.1997.7590.

Cheng, F., Dupont, V., Twigg, M.V., 2017. Direct sereduction of nickel catalyst with model bio-compounds. Appl. Catal. B 200, 121–132. http://dx.doi.org/10.1016/j.apcatb.2016.06.044.

Cheng, Z., Wu, Q., Li, J., Zhu, Q., 1996. Effects seof promoters and preparation procedures on reforming of methane with carbon dioxide over Ni/Al_2O_3 catalyst. Catal. Today 30, 147–155. http://dx.doi.org/10.1016/0920-5861(95)00005-4.

Christensen, K.O., Chen, D., Lødeng, R., Holmen, A., 2006. Effect seof supports and Ni crystal size on carbon formation and sintering during steam methane reforming. Appl. Catal. A 314, 9–22. http://dx.doi.org/10.1016/j.apcata.2006.07.028.

de Diego, L.F., Ortiz, M., Adánez, J., García-Labiano, F., Abad P. Gayán, P., 2008. Synthesis segas generation by chemical-looping reforming in a batch fluidized bed reactor using Ni-based oxygen carriers. Chem. Eng. J. 144, 289–298. http://dx.doi.org/10.1016/j.cej.2008.06.004.

Dueso, C., Abad, A., García-Labiano, F., De Diego, L.F., Gayán, P., Adánez, J., Lyngfelt, A., 2010. Reactivity seof a NiO/Al_2O_3 oxygen carrier prepared by impregnation for chemical-looping combustion. Fuel 89, 3399–3409. http://dx.doi.org/10.1016/j.fuel.2010.03.043.

Dueso, C., Ortiz, M., Abad, A., García-Labiano, F., De Diego, L.F., Gayán, P., Adánez, J., 2012. Reduction seand oxidation kinetics of nickel-based oxygen-carriers for chemical-looping combustion and chemical-looping reforming. Chem. Eng. J. 188, 142–154. http://dx.doi.org/10.1016/j.cej.2012.01.124.

Espinose, J., Caillerie, D., Kermarec, M., Clause, O., 1995. Impregnation seof y-Alumina with Ni (II) or Co (II) Ions at Neutral pH : Hydrotalcite-Type Coprecipitate Formation and Characterization. J. Am. Chem. Soc. 117, 11471–11481. http://dx.doi.org/10.1021/ja00151a010.

Feng, J.T., Lin, Y.J., Evans, D.G., Duan, X., Li, D.Q., 2009. Enhanced semetal dispersion and hydrodechlorination properties of a Ni/Al_2O_3 catalyst derived from layered double hydroxides. J. Catal 266, 351–358. http://dx.doi.org/10.1016/j.jcat.2009.07.001.

Gayán, P., de Diego, L.F., García-Labiano, F., Adánez, J., Abad, A., Dueso, C., 2008. Effect seof support on reactivity and selectivity of Ni-based oxygen carriers for chemical-looping combustion. Fuel 87, 2641–2650. http://dx.doi.org/10.1016/j.fuel.2008.02.016.

Gayán, P., Dueso, C., Abad, A., . Adanez, J., de Diego, L.F., García-Labiano, F., 2009. $NseiO/Al_2O_3$ oxygen carriers for chemical-looping combustion prepared by impregnation and deposition-precipitation methods. Fuel 88, 1016–1023. http://dx.doi.org/10.1016/j.fuel.2008.12.007.

Hossain, MM., de Lasa, H.I., 2007. Reactivity seand stability of $Co-Ni/Al_2O_3$ oxygen carrier in multicycle CLC. AIChE J. 53, 1817–1829. http://dx.doi.org/10.1002/aic.11188.

Hossain, M.M., Sedor, K.E., de Lasa, H.I., 2007. Oxygen secarrier for fluidized bed chemical-looping combustion: Desorption kinetics and metal–support interaction. Chem. Eng. Sci. 62, 5464–5472. http://dx.doi.org/10.1016/j.ces.2006.12.066.

Jin, H., Okamoto, T., Ishida, M., 1998. Development seof a Novel Chemical-Looping Combustion: Synthesis of a Looping Material with a Double Metal Oxide of CoO-NiO. Energy Fuels. 12, 1272–1277.

Li, M., Fan, G., Qin, H., Li, F., 2012. Investigation seof the structure and catalytic performance of highly dispersed Ni-based catalysts for the growth of carbon nanostructures. Ind. Eng. Chem. Res. 51, 11892–11900. http://dx.doi.org/10.1021/ie3008659.

Lucrédio, A.F., Assaf, E.M., 2006. Cobalt secatalysts prepared from hydrotalcite precursors and tested in methane steam reforming. J. Power Sources 159, 667–672. http://dx.doi.org/10.1016/j.jpowsour.2005.10.108.

Mattisson, T., . Johansson, M., Lyngfelt, A., 2006. The seuse of NiO as an oxygen carrier in chemical-looping combustion. Fuel 85, 736–747. http://dx.doi.org/10.1016/j.fuel.2005.07.021.

McBride, B.J., Gordon, S., 1994. Computer Program for Calculation of Complex Chemical Equilibrium Compositions and Applications. NASA Ref. Publ, 1311: 184. doi:NASA RP-1311.

Neimark, A.V., Kheifez, L.I., Fenelonov, V.B., 1981. Theory seof preparation of supported catalysts. Ind. Eng. Chem. Prod. Res. Dev. 20, 439–450. http://dx.doi.org/10.1021/i300003a006.

Noorman, S., van Sint Annaland, M., Kuipers, 2007. Packed seBed Reactor Technology for Chemical-Looping Combustion. Ind. Eng. Chem. Res. 46, 4212–4220. http://dx.doi.org/10.1021/ie061178i.

Noorman, S., van Sint Annaland, M., Kuipers, JAM., 2010. Experimental sevalidation of packed bed chemical-looping combustion. Chem. Eng. Sci. 65, 92–97. http://dx.doi.org/10.1016/j.ces.2009.02.004.

Peng, H.X., Fan, Z., Evans, J.R.G., 2001. Cellular searrays of alumina fibres. J. Mater. Sci. 36, 1007–1013. http://dx.doi.org/10.1023/A:1004892310835.

Pimenidou, P., Rickett, G., Dupont, V., Twigg, M.V., 2010. Chemical selooping reforming of waste cooking oil in packed bed reactor. Bioresour. Technol. 101, 6389–6397. http://dx.doi.org/10.1016/j.biortech.2010.03.053.

Protasova, L., Snijkers, F., 2016. Recent sedevelopments in oxygen carrier materials for hydrogen production via chemical looping processes. Fuel 181, 75–93. http://dx.doi.org/10.1016/j.fuel.2016.04.110.

Quddus, M.R., Hossain, M., De Lasa, H.I., 2013. Ni sebased oxygen carrier over $gama-Al_2O_3$ for chemical looping combustion: Effect of preparation method on metal support interaction. Catal. Today 210, 124–134. http://dx.doi.org/10.1016/j.cattod.2013.02.005.

Radcliffe, S.W., Hickman, R.G., 1975. Diffusive secatalytic combustors. J. Inst. Fuels. 48, 208–214.

Reichelt, E., Heddrich, MP., Jahn, M., Michaelis, A., 2014. Fiber sebased structured materials for catalytic applications. Appl. Catal. A 476, 78–90. http://dx.doi.org/10.1016/j.apcata.2014.02.021.

Reichelt, E., Jahn, M., 2017. Generalized secorrelations for mass transfer and pressure drop in fiber-based catalyst supports. Chem. Eng. J. 325, 655–664. http://dx.doi.org/10.1016/j.cej.2017.05.119.

Rydén, M., Ramos, P., 2012. H_2 production with CO_2 capture by sorption enhanced chemical-looping reforming using NiO as oxygen carrier and CaO as CO_2 sorbent. Fuel Process. Technol. 96, 27–36. http://dx.doi.org/10.1016/j.fuproc.2011.12.009.

Ryu, H-J., Bae, D-H., Han, K-H., Lee, S-Y., Jin, G-T., Choi, J-T., 2001. Oxidation seand reduction characteristics of oxygen carrier particles and reaction kinetics by unreacted core model, Korean J. Chem. Eng. 18, 831–837. http://dx.doi.org/10.1007/BF02705604.

Sadamori, H., 1999. Application seconcepts and evaluation of small-scale catalytic combustors for natural gas. Catal. Today 47, 325–338. http://dx.doi.org/10.1016/S0920-5861(98)00314-9.

Song, Q., Liu, W., Bohn, C.D., Harper, R.N., Sivaniah, E., Scott, SA., Dennis, J.S., 2013. A sehigh performance oxygen storage material for chemical looping processes with CO_2 capture. Energy Environ. Sci. 6, 288–298. http://dx.doi.org/10.1039/C2EE22801G.

Tang, M., Xu, L., Fan, M., 2015. Progress sein oxygen carrier development of methane-based chemical-looping reforming: A review. Appl. Energy 151, 143–156. http://dx.doi.org/10.1016/j.apenergy.2015.04.017.

Trimm, D.L., Lam, C.W., 1980a. The secombustion of methane on platinum-alumina fibre catalyst - II. Chem. Eng. Sci. 35, 1731–1739.

Trimm, D.L., Lam, C.W., 1980b. The secombustion of methane on platinum-alumina fibre catalysts-I. Kinetics Mech. Chem. Eng. Sci. 35, 1405–1413. http://dx.doi.org/10.1016/0009-2509(80)85134-7.

Xu, Z., Wang, N., Chu, W., Deng, J., Luo, S., 2015. In sesitu controllable assembly of layered-double-hydroxide-based nickel nanocatalysts for carbon dioxide reforming of methane. Catal. Sci. Technol. 5, 1588–1597. http://dx.doi.org/10.1039/C4CY01302F.

You, X., Wang, X., Ma, Y., Liu, J., Liu, W., Xu, X., Peng, H., Li, C., Zhou, W., Yuan, P., Chen, X., 2014. $Nsei-Co/Al_2O_3$ Bimetallic Catalysts for CH_4 Steam Reforming: Elucidating the Role of Co for Improving Coke Resistance. ChemCatChem. n/a–n/a.. http://dx.doi.org/10.1002/cctc.201402695.

Zafar, Q., Mattisson, T., Gevert, B., 2005. Integrated sehydrogen and power production with CO_2 capture using chemical-looping reforming-Redox reactivity of particles of CuO, Mn_2O_3, NiO, and Fe_2O_3 using SiO_2 as support. Ind. Eng. Chem. Res 44, 3485–3496. http://dx.doi.org/10.1021/ef0501389.

Zafar, Q., Mattisson, T., Gevert, B., 2006. Redox seinvestigation of some oxides of transition-state metals Ni, Cu, Fe, and supported on SiO_2 and $MgAl_2O_4$. Energy Fuels 20, 34–44. http://dx.doi.org/10.1021/ef0501389.

Zhao, H., Draelants, D.J., Baron, G.V., 2000. Preparation seand characterisation of nickel-modified ceramic filters. Catal. Today 56, 229–237. http://dx.doi.org/10.1016/S0920-5861(99)00280-1.

Zhou, W., Wang, Q., Li, J., Tang, Y., Huang, Z., Zhang, J., Lu, Q., 2015. Hydrogen seproduction from methanol steam reforming using porous copper fiber sintered felt with gradient porosity. Int. J. Hydrogen Energy 40, 244–255. http://dx.doi.org/10.1016/j.ijhydene.2014.10.139.